ACS APPLIED MATERIALS & INTERFACES

Research Article

www.acsami.org

Improving Electrical Conductivity in Polycarbonate Nanocomposites Using Highly Conductive PEDOT/PSS Coated MWCNTs

Jian Zhou and Gilles Lubineau*

King Abdullah University of Science and Technology (KAUST), Physical Science and Engineering Division, COHMAS Laboratory, Thuwal 23955-6900, Saudi Arabia

ABSTRACT: We describe a strategy to design highly electrically conductive polycarbonate nanocomposites by using multiwalled carbon nanotubes (MWCNTs) coated with a thin layer of poly(3,4-ethylenedioxythiophene)/poly(styrenesulfonate), a conductive polymer. We found that this coating method improves the electrical properties of the nanocomposites in two ways. First, the coating becomes the main electrical conductive path. Second, the coating promotes the formation of a percolation network at a low filler concentration (0.3 wt %). To tailor the electrical properties of the conductive polymer coating, we used a polar solvent ethylene glycol, and we can tune the final properties of the nanocomposite by controlling the concentrations of the elementary constituents or the intrinsic properties of the conductive polymer coating. This very flexible technique allows for tailoring the properties of the final product.

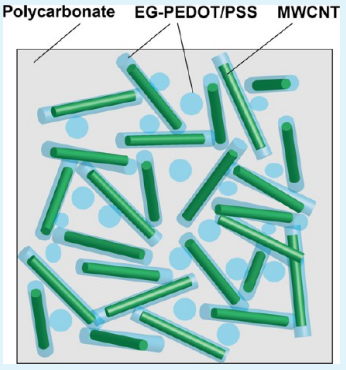

KEYWORDS: *PEDOT/PSS, MWCNTs, polycarbonate, ethylene glycol, electrical conductivity*

INTRODUCTION

Good mechanical properties and thermal stability make polycarbonate (PC) a very successful engineering thermoplastic in aeronautical applications.[1] Yet, improving the electrical properties of PC is necessary for some applications for which electrical charge mitigation is a key design constraint. Examples of such applications include lightning protection and electromagnetic shielding. Many efforts have been directed toward functionalizing insulating polymers with electrically conductive nanofillers.[2−4] Among other emerging technologies, carbon nanotube (CNT) reinforced polymeric composites demonstrate excellent electrical properties. Their applications range widely from displays and batteries to solar cells and automotive and aerospace structures.[5−11]

Achieving good dispersion of the nanofillers is essential to ensuring improved electrical conductivity in PC. Various types of dispersants have been used to disperse CNTs in polymers, including surfactants, polymers, biomolecules, and inorganic nanoparticles.[12−16] Most of these dispersants are electrical insulators. Another interesting approach is to use a conductive polymer such as poly(3,4-ethylenedioxythiophene)/poly(styrenesulfonate) (PEDOT/PSS). The PEDOT backbone contains aromatic thiophene rings, which enable strong $\pi-\pi$ stacking interactions with hybridized carbon on the surface of the CNTs. It helps to separate the agglomerated CNTs and therefore improves the dispersion.[17,18] This is a noncovalently method to reduce nanofiller aggregation,[19] making this method much less destructive than covalent methods. PSS acts as a surfactant to disperse the CNTs, and its long molecular chain wraps around the CNTs to separate them from each other.[20−22]

On top of improving the dispersion of the nanofillers, PEDOT/PSS can also be used to counterbalance the insulating effect of the bulk polymer matrix.[23,24] Ma et al. showed that the conductivity of SWCNT networks could be dramatically improved by 2 orders of magnitude using in situ polymerization of a highly conductive self-doped conducting polymer (polyaniline boronic acid) around and along the CNTs.[25] Kyrylyuk and co-workers reported a latex-based route involving the mixing of fibrous SWCNTs and spherical PEDOT/PSS latex particles, which allowed the value of the percolation threshold in the nanocomposite to be controlled.[17,18,26] The $\pi-\pi$ interaction also helps to form conductive phases between the polymer matrix and carbon nanofillers, which improves the electrical properties of the resulting bulk polymer nanocomposites.

It is worth noting that the electrical conductivity of PEDOT/PSS can be greatly enhanced by solvent treatment using a polar solvent such as ethylene glycol (EG).[27,28] Our previous studies showed that the electrical conductivity of PEDOT/PSS (Clevios P)-coated paper can be enhanced by 3 orders of magnitude by EG treatment.[29−32] A mechanism has been proposed to explain the enhancement of the electrical conductivity by EG based on the change in conformation of the PEDOT backbone from a coiled to a linear of extended coil structure.[33] This mechanism suggests that a final product can be tuned by controlling the conductivity of the conductive polymer.

Here, we use MWCNTs as a nanofiller to enhance the electrical properties of PC. Without additional modification, the filler−filler junctions of MWCNTs are covered with insulating

Received: March 31, 2013
Accepted: June 12, 2013
Published: June 12, 2013

   dx.doi.org/10.1021/am4011622 | ACS Appl. Mater. Interfaces 2013, 5, 6189−6200

Table 1. Summary of All Investigated Nanocomposite Configurations

samples	MWCNT loading with respect to PC (wt %)	EG loading with respect to PEDOT/PSS (wt %)	PEDOT/PSS or EG-PEDOT/PSS loading with respect to PC (wt %)
PC	0	0	0
MWCNT/PC	0.1	0	0
MWCNT/PC	0.3	0	0
MWCNT/PC	0.5	0	0
MWCNT/PC	1	0	0
MWCNT/PC	2	0	0
MWCNT/(PEDOT/PSS)/PC	0.1	0	0.13
MWCNT/(PEDOT/PSS)/PC	0.3	0	0.39
MWCNT/(PEDOT/PSS)/PC	0.5	0	0.65
MWCNT/(PEDOT/PSS)/PC	1	0	1.3
MWCNT/(PEDOT/PSS)/PC	2	0	2.6
MWCNT/(EG-PEDOT/PSS)/PC	0.1	5	0.13
MWCNT/(EG-PEDOT/PSS)/PC	0.3	5	0.39
MWCNT/(EG-PEDOT/PSS)/PC	0.5	5	0.65
MWCNT/(EG-PEDOT/PSS)/PC	1	5	1.3
MWCNT/(EG-PEDOT/PSS)/PC	2	5	2.6
MWCNT/(EG-PEDOT/PSS)/PC	0.3	1	0.39
MWCNT/(EG-PEDOT/PSS)/PC	0.3	3	0.39
MWCNT/(EG-PEDOT/PSS)/PC	0.3	7	0.39
MWCNT/(EG-PEDOT/PSS)/PC	0.5	1	0.65
MWCNT/(EG-PEDOT/PSS)/PC	0.5	3	0.65
MWCNT/(EG-PEDOT/PSS)/PC	0.5	7	0.65
MWCNT/(EG-PEDOT/PSS)/PC	0.5	5	0.195
MWCNT/(EG-PEDOT/PSS)/PC	0.5	5	0.325
MWCNT/(EG-PEDOT/PSS)/PC	0.5	5	0.455
MWCNT/(EG-PEDOT/PSS)/PC	1	5	0.39
MWCNT/(EG-PEDOT/PSS)/PC	1	5	0.65
MWCNT/(EG-PEDOT/PSS)/PC	1	5	0.91

PC. Hence, we enhanced the filler−filler junctions by coating the MWCNTs with a nanolayer of highly conductive polymer PEDOT/PSS using a latex-based route. We produced MWCNT/PC composites using this latex-based approach by directly mixing PEDOT/PSS aqueous dispersions of exfoliated MWCNTs with PC. We were able to vary multiple parameters, including the content of the nano filler as well as the content and the intrinsic properties of the conductive polymer to tailor the electrical properties of the final product.

We first report on a preliminary study of the dispersion, morphological and conductive properties of the MWCNT/(PEDOT/PSS) polymer blend that we subsequently used to dope the PC. We describe the intrinsic improvements in the electrical properties of PEDOT/PSS by EG treatment. Then, we describe how this MWCNT/(PEDOT/PSS) arrangement is used to dope PC to create a low-resistivity bulk thermoplastic material. We characterize the properties of the resulting three-phase material in different MWCNT and PEDOT/PSS configurations to evaluate the potential of this approach. We thus provide a systematic guide to designing a downstream process that produces nanocomposites with tunable electrical properties.

EXPERIMENTAL SECTION

Materials. PC in fine granular form (Lexan ML9103-111T) was provided by Sabic innovative plastics. Carboxyl group (−COOH) functionalized MWCNTs were purchased from CheapTubes, Inc., with over 95 wt % purity and containing 2.56 wt % of COOH groups. The true density of these MWCNTs was 2.1 g/cm^3. The PEDOT/PSS aqueous dispersion (Clevios PH1000) was purchased from HC Starck, Inc. EG, dichloromethane (DCM), and dimethylformamide (DMF) were purchased from Sigma-Aldrich.

Preparation of the Conductive Blend. A comprehensive study was conducted to optimize a conductive blend based on both the treated conductive polymer and the MWCNTs. This conductive blend (used in the following section as an additive to the PC) was made of exfoliated MWCNTs in a EG-treated PEDOT/PSS (EG-PEDOT/PSS) solution. First, the effect of EG treatment on the intrinsic conductivity of PEDOT/PSS was confirmed and related to a rearrangement of the conformation of PEDOT/PSS. To optimize the EG loading to be used, five weight percentage configurations of the proportion of EG added to PEDOT/PSS were investigated: 0, 1, 3, 5, and 7 wt %. The effect of EG treatment was evaluated on both pure PEDOT/PSS and MWCNT/(PEDOT/PSS) blends. In each configuration, the EG-PEDOT/PSS blend was first stirred for 2 h at room temperature. Then, to the samples to which MWCNTs were added, 0.5 wt % of MWCNTs were added to 10 mL of these different solutions and 10 mL of distilled water. The exfoliation of the MWCNTs was performed using a Brason 8510 bath sonicator (Thomas Scientific) for 1 h, followed by an Ultrasonic processor (Cole-Parmer) at 20 kHz and 500 W for 15 min in an ice water bath to prevent extensive heating and damage of the MWCNTs.

Based on our observations (presented below), we determined that a 5 wt % EG load would be used in all subsequent samples. We prepared pristine PEDOT/PSS films, EG-PEDOT/PSS films, MWCNT/(PEDOT/PSS) films, and MWCNT/(EG-PEDOT/PSS) films by spin-coating these dispersions on glass substrates at a speed of 5000 rpm/min for 40s. These films were subsequently annealed on a hot plate at 120 °C for 30 min at ambient atmosphere. Glass substrates with areas of 2.5 × 2.5 cm^2 were pretreated with oxygen plasma via a PlasmaLab 100 system (Oxford Instruments) for 15 min before spin-coating; this process will help to remove the dust and improve wettability of the glass substrate and finally improve the uniformity of the spin-coated films.

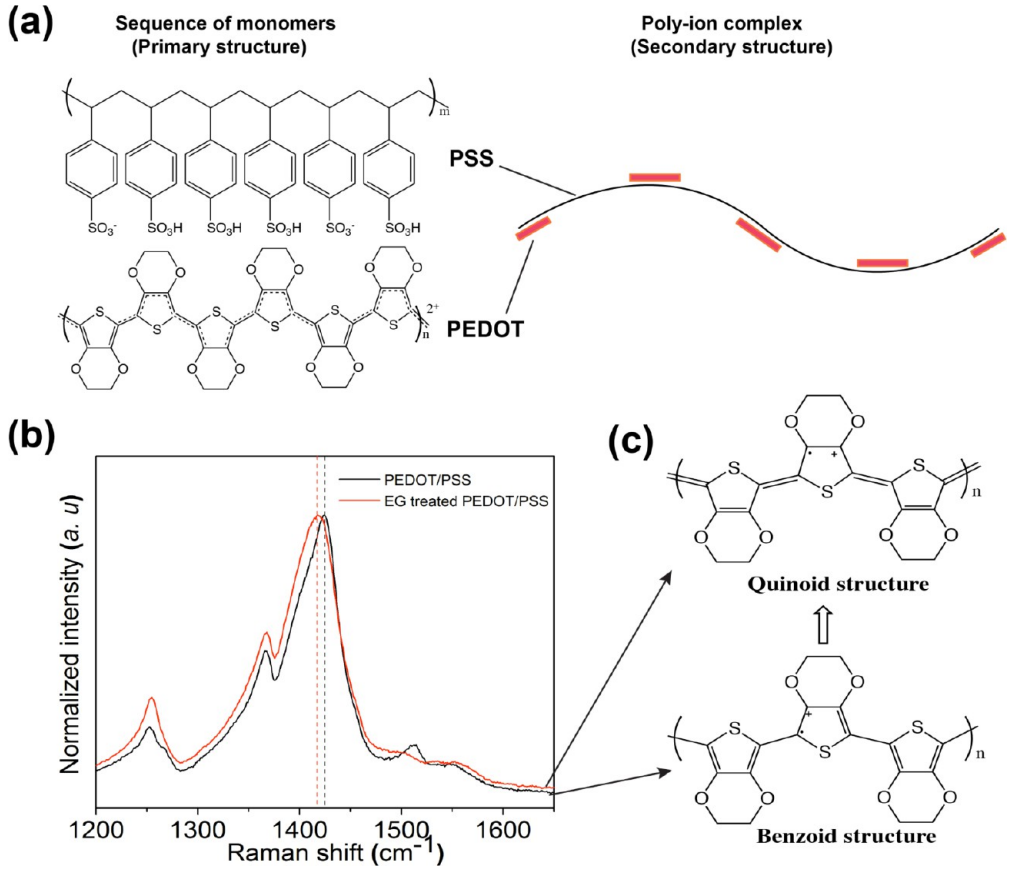

Figure 1. (a) Primary and secondary structures of PEDOT/PSS, (b) Raman spectra of pristine PEDOT/PSS and EG-PEDOT/PSS at an excitation wavelength of 632.8 nm, and (c) Scheme of the transformation of the PEDOT chain from a benzoid to a quinoid structure by EG treatment.[33]

Preparation of the PC-Based Nanocomposites. PC was dissolved in DCM by stirring for 5 h at room temperature and then blended with the surface-modified MWCNTs. The resulting mixture of MWCNT/(PEDOT/PSS)/PC or MWCNT/(EG-PEDOT/PSS)/PC was first stirred for 12 h at room temperature, and then film samples were prepared via a cast-coating method. The porous casted films were formed into 0.20 mm thick rectangular samples by a hydraulic hot press (Pinette Emidecau Industries) at 240 °C and 7 bar for 30 min. Just before the hot pressing, the porous film was heated for 1 h until it reached 240 °C. MWCNT/PC nanocomposites without using PEDOT/PSS were also prepared for comparison. All sample compositions are given in Table 1.

Characterizations. Sheet resistances (R_s) of the spin-coated films were measured via a CMT-SR2000N four-probe system with a probe space of 1 mm (Materials Development Corporation). The volume resistivity (ρ) of the thin film was defined as

$$\rho = R_s t = Kt\frac{U}{I} \quad (1)$$

Considering that all films had a thickness t in the range of 40−100 nm (well below half the probe spacing), we used the classical thin film correction constant K which is defined as

$$K = \frac{\pi}{In(2)} = 4.532 \quad (2)$$

where U (V) is the measured voltage, and I (A) is the prescribed current.[34] On each sample, we measured the resistivity at 10 different locations on the sample, then the measured values were averaged. The thickness of each film was measured with a Dektak 8 surface profilometer (Veeco Instruments Inc.). As far as the PC-based nanocomposites were concerned, the surface and volume resistivities of the nanocomposite samples were measured according to ASTM D257 using a Keithley 6517B electrometer equipped with a 8009 test fixture (Keithley Instruments Inc.). Each specimen was a compression-molded rectangular sample with dimensions of 100 × 100 × 0.20 mm^3. Five samples were tested and averaged for each formulation.

Transmission electron microscopy (TEM) images were taken with a Tecnai Spirit T12 (FEI Company) instrument on both aqueous dispersions and nanocomposites at an accelerating voltage of 120 kV. TEM samples of the dispersions were prepared by dropping one drop of as-prepared aqueous solution (0.5 wt %) onto a 3 mm, 300 mesh copper grid (Pacific Grid Tech). These samples were then air-dried at room temperature before observation. To prepare TEM samples of the nanocomposite, ultrathin sections of about 100 nm were cut using a EM UC6 microtome (Leica Microsystems) equipped with a glass knife and placed on a 3 mm, 300 mesh copper grid. Scanning electronic microscopy (SEM) was performed using a Quanta 600 (FEI Company) instrument. Atomic force microscopy (AFM) images of spin-coated films were taken using a Agilent 5400 (Agilent Technologies) instrument in the tapping mode under ambient condition. Raman spectra were collected using a LabRAM Aramis Raman spectrometer (Horiba, Ltd.) on spin-coated films. Fourier transform infrared (FTIR) spectra of samples were obtained using an Nicolet iS10 spectrometer (Thermo Fisher Scientific, Inc.).

RESULTS AND DISCUSSION

Effect of EG on PEDOT/PSS. As EG will be used in the final product to tailor the electrical conductivity of the conductive polymer layer, this short preliminary study intends to exactly quantify its effects. We also checked that the actual modification obtained in our system is consistent with explanations already provided in the literature.[29,30,35−37] PEDOT/PSS is commercially available as colloidal gel particles in an aqueous dispersion. The gel particles have a hierarchical structure as shown in Figure 1a. The sequence of monomer

dx.doi.org/10.1021/am4011622 | ACS Appl. Mater. Interfaces 2013, 5, 6189−6200

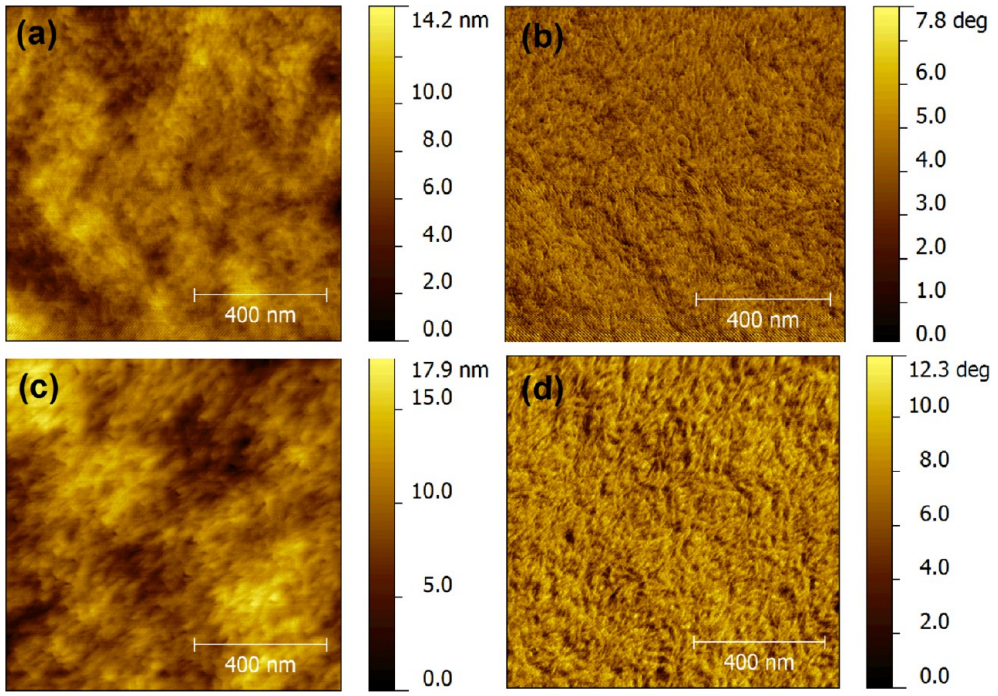

Figure 2. (a, c) AFM height images of pristine PEDOT/PSS film and EG-PEDOT/PSS films films (EG loading in PEDOT/PSS: 5 wt %); (b, d) AFM phase images of pristine PEDOT/PSS film and EG treated PEDOT/PSS films. All the images are 1 μm × 1 μm.

units of PEDOT and PSS (primary structure) forms a polyion complex (secondary structure) through electrostatic interactions between sulfonyl hydroxide ($-SO_3H$) and the PEDOT backbone. The hydrophobic PEDOT molecules aggregated to form physical cross-links with the PSS chains. Thus, the polyion complex can easily disperse in water as colloidal gel particles with diameters of several tens of nanometers.[37]

Many reports showed that adding polar solvent into a PEDOT/PSS dispersion significantly improved its electrical conductivity.[29−32,35,36] Ouyang and Okuzaki demonstrated conductivity enhancement by adding EG into PEDOT/PSS and proposed a mechanism of conformational change of PEDOT from a benzoid structure to a quinoid structure for the conductivity enhancement.[37,38] Recently, Takano et al. found a correlation between electrical conductivity and EG-induced crystallinity of PEDOT.[39] Based on these studies, the electrical properties of PEDOT/PSS can be adjusted by varying the amount of polar solvent added.[40] As a preliminary experiment, we confirmed this result in our EG-PEDOT/PSS films. For 5 wt % EG loaded into PEDOT/PSS, the volume resistivity of the PEDOT/PSS film decreased by 3 orders of magnitude from 1.47 ± 0.67 Ω·cm to (2.51 ± 0.2) × 10^{-3} Ω·cm (Figure 5). To explain this change in volume resistivity, we used Raman microscopy to investigate the molecular changes in PEDOT/PSS caused by EG. Pristine PEDOT/PSS had a strong peak at 1423 cm^{-1}, which was assigned to symmetric $C_\alpha = C_\beta$ stretching deformation in the aromatic thiophene ring. However, this peak red-shifted to 1417 cm^{-1} from a benzoid structure to a quinoid structure due to the EG treatment (Figure 1b and c).[33] The relative intensity of asymmetric $C_\alpha = C_\beta$ stretching at 1517 cm^{-1} for EG treated PEDOT/PSS was also lower than that of pristine PEDOT/PSS, indicating a predominately in-plane backbone for the doped structure.[29,41,42]

AFM images were taken to investigate the possible changes in the morphology and the correlation between morphology and conductivity. They are presented in Figure 2. The height images show that both the pristine PEDOT/PSS film and EG-PEDOT/PSS films are reasonably smooth with a root-mean-square (rms) roughness of 1.6 and 2.6 nm, respectively. But grains with elongated structures exist on the EG-PEDOT/PSS film. The grains were seen to be more aggregated, and they increased in size after EG treatment (Figure 2c). The phase image shows weak phase separation between PEDOT and PSS in the pristine PEDOT/PSS film. However, there was an increased phase separation between PEDOT and PSS in the EG-PEDOT/PSS film, suggesting that the conformation of PEDOT changed from a coiled to a linear or extended coil structure owing to the treatment PEDOT/PSS by EG. As the benzoid structure is the favored structure for a coil conformation, while the quinoid structure is favored for a linear or expanded-coil conformation, it is understandable that the EG-treated PEDOT/PSS chains with linear or expanded-coil conformations have high charge-carrier mobility. The way charges are transported among the highly conducting PEDOT-rich grains determines the overall conductivity of a PEDOT/PSS film.[35,37,43] As a result, the PEDOT-rich chains with linear structures, larger grain sizes, and lower intergrain hoping result in thinner PSS barriers and finally lead to higher conductivity.

Characterization of the MWCNT/(EG-PEDOT/PSS) Conductive Blend. The MWCNT dispersion was characterized by TEM as shown in Figure 3a (the weight ratio of EG-PEDOT/PSS to MWCNT) is fixed at 1.3 for Figure 3a and b). The TEM images show that the MWCNTs were well dispersed as individually separated nanotubes in EG-PEDOT/PSS. The average diameter of these coated tubes was 19.6 ± 4.4 nm. A high magnification TEM image shows that a very thin EG-PEDOT/PSS layer coated the outer wall of MWCNTs with an unsmooth surface (Figure 3b). The thickness of the coated layer typically ranged from 2 to 4 nm. Yet, we suspect that there was a gradient of crystallinity of the PEDOT/PSS from the CNT surface due to the following reason: PEDOT has a strong $\pi-\pi$ stacking interactions between the surfaces of the

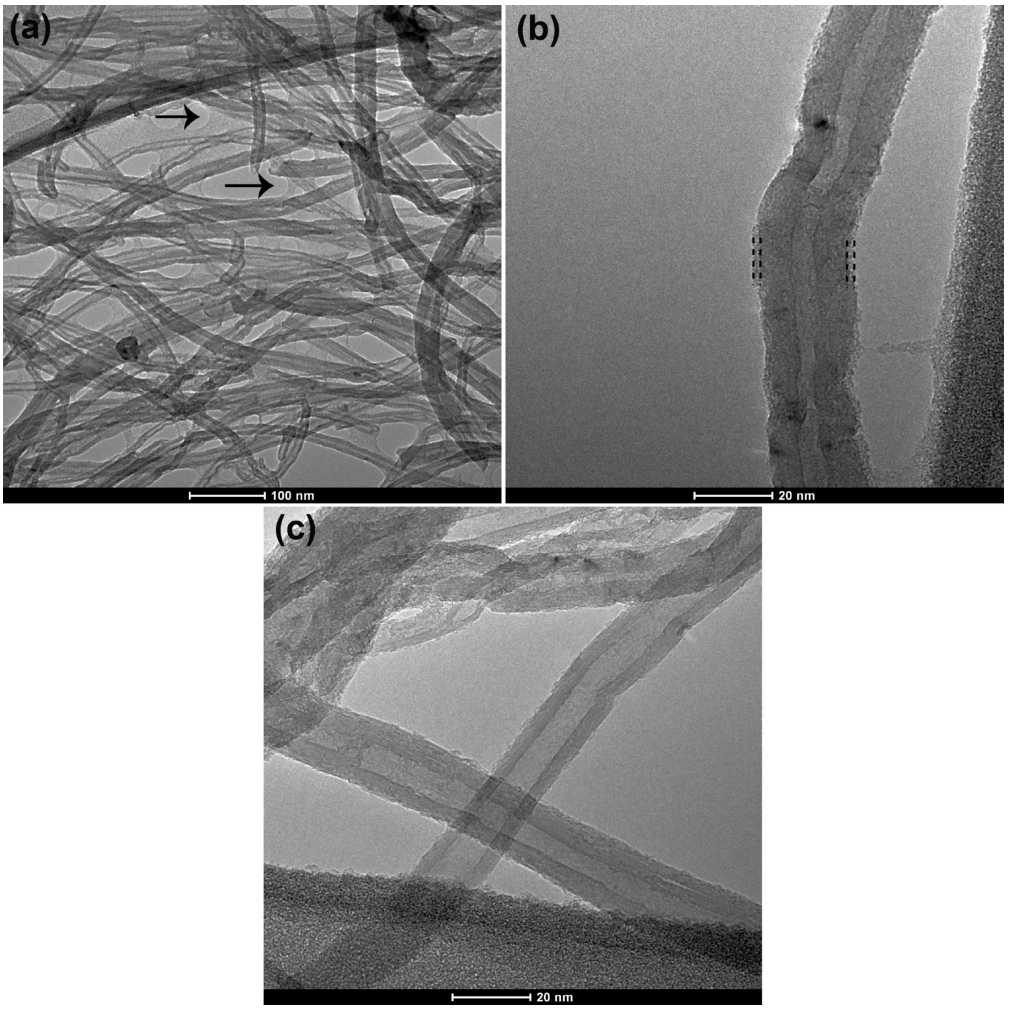

Figure 3. (a) Low magnification TEM images of EG-PEDOT/PSS dispersed MWCNTs (the arrows have been added to indicate EG-PEDOT/PSS between the MWCNTs that tends to separate MWCNT bundles). (b) High magnification TEM image of EG-PEDOT/PSS dispersed MWCNTs (the dotted lines have been added as a visual guide to locate the EG-PEDOT/PSS films coated layer). (c) TEM image of DMF-dispersed MWCNTs. In (a) and (b), PEDOT/PSS contains 5 wt % EG. The weight ratio of EG-PEDOT/PSS and MWCNTs is fixed at 1.3:1.

MWCNTs and the thiophene rings on PEDOT; the amorphous PSS will be in the outer part of PEDOT/PSS coated MWCNTs. In this case, we should consider that the observed 2−4 nm thickness observed by TEM for the EG-PEDOT/PSS coated layer was a lower bound value mainly corresponding to the outer amorphous phase; the actual thickness might be slightly larger. By contrast, DMF-dispersed MWCNTs were also observed by TEM. These uncoated MWCNTs had relatively smooth surfaces compared with the EG-PEDOT/PSS coated MWCNTs (Figure 3c). The average diameter of the MWCNTs measured from TEM was 12.1 ± 2.5 nm, which was in the range of values provided by the supplier (8−15 nm).

In the SEM images of DMF-dispersed MWCNTs (Figure 4a) and MWCNT/(EG-PEDOT/PSS) spin-coated films (Figure 4b−e), we can also easily see monodispersed MWCNTs. Moreover, we found that the apparent diameters of the EG-PEDOT/PSS coated MWCNTs could be adjusted by changing the weight ratio of EG-PEDOT/PSS and MWCNTs (from 0.39:1, 0.65:1, 0.91:1, 1.3:1; see Figure 4f). However, the theoretical calculated thicknesses of the coated EG-PEDOT/PSS layer were 1.7, 2.8, 3.9, and 5.6 nm, respectively (estimated by the given surface area of MWCNTs and the weight of PEDOT/PSS). These theoretical values compare well with the TEM-measured thickness for the 1.3:1 EG-PEDOT/PSS:MWCNT weight ratio (theoretical thickness, 5.6 nm; TEM measured thickness, 3.7 nm; the TEM value being a bit smaller due to the crystallinity gradient as noted in the previous paragraph). The thicknesses measured in the SEM images are two times larger than the theoretical values (Figure 4f). This difference could be due to charge-contrast imaging of SEM, which inherently distorts the MWCNT thickness, as the average diameter of DMF-dispersed MWCNTs measured from SEM was 16 ± 4 nm, which was about 4 nm thicker than the value measured from the TEM image. Diameters of MWCNTs measured from SEM images still give us an indication that MWCNTs could be coated by EG-PEDOT/PSS layers of different thicknesses. The PEDOT/PSS stays strongly absorbed on the MWCNT surface even during high speed spin-coating at 5000 rpm/min. This coating process is simply realized by exfoliation of the MWCNTs in EG-PEDOT/PSS by a bath sonicator and tip sonicator. The good coating of the PEDOT/PSS layer on MWCNTs could be attributed to the following two related reasons: (1) strong $\pi-\pi$ stacking interactions between the outer surfaces of the MWCNTs and the thiophene rings on PEDOT and (2) long-chain PSS segments in the

dx.doi.org/10.1021/am4011622 | ACS Appl. Mater. Interfaces 2013, 5, 6189−6200

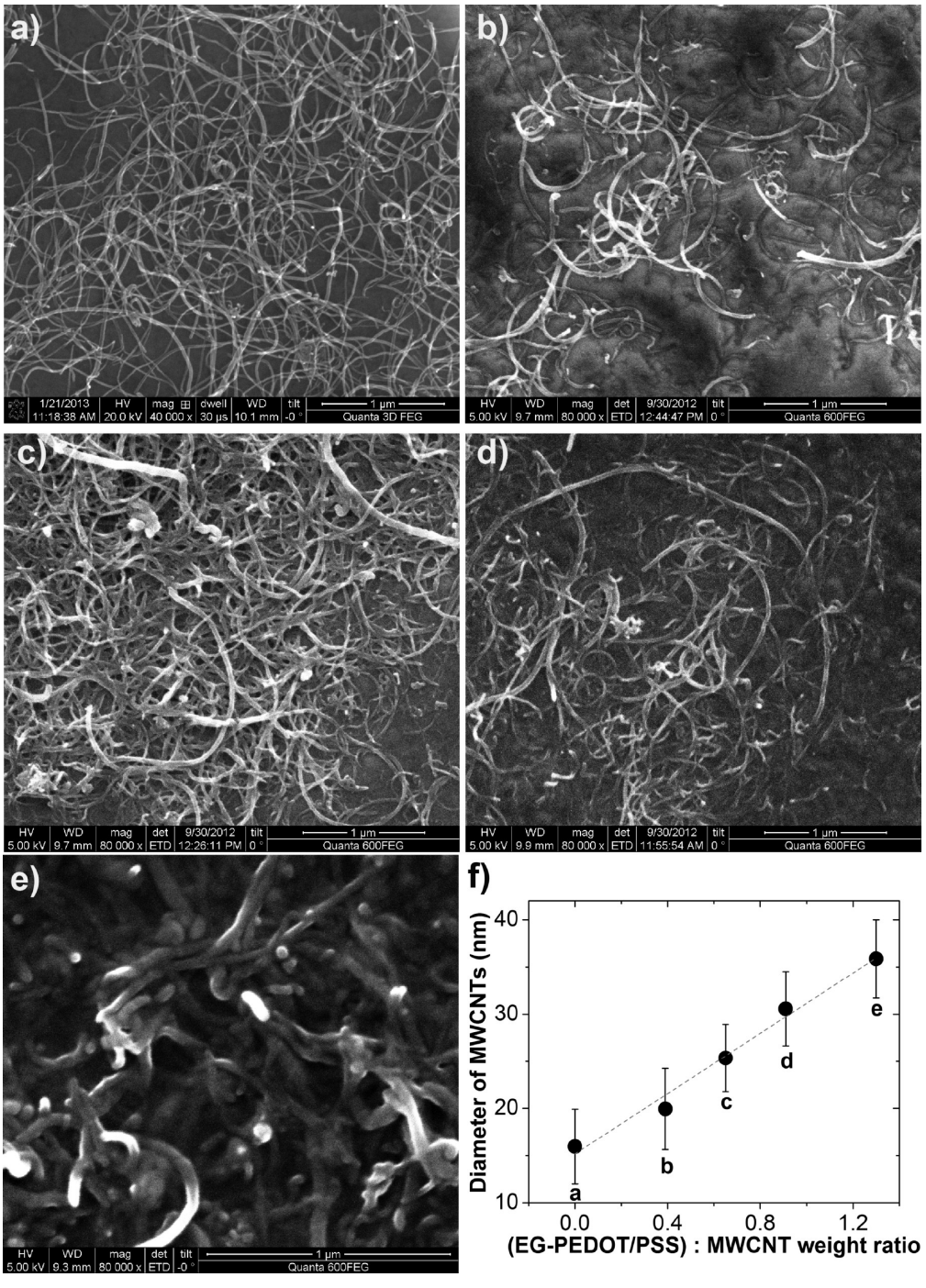

Figure 4. (a) SEM image of DMF-dispersed MWCNTs. (b–e) SEM image of spin-coated MWCNT/(EG-PEDOT/PSS) films with different (EG-PEDOT/PSS): MWCNT weight ratios (b, 0.39:1; c, 0.65:1; d, 0.91:1; e, 1.3:1). (f) Diameter of PEDOT/PSS-coated MWCNTs with different configurations (diameters are measured from SEM images from (a) to (e)).

PEDOT/PSS compound playing an important role in wrapping MWCNTs.

Since we confirmed that MWCNTs could be efficiently coated by a thin EG-PEDOT/PSS layer, we investigated the polar solvent treatment route. By controlling the EG loading, we tailored the electrical properties of the MWCNT/(EG-PEDOT/PSS) conductive blend. Figure 5 shows that the volume resistivity of EG-PEDOT/PSS decreases monotonically with increasing the EG content. Enhancement of the volume resistivity tends to slow down beyond the addition of 5 wt % EG into the PEDOT/PSS solution. Similar results have been reported for another type of PEDOT/PSS (Clevios P) in which EG loading over 7 wt % normally decreased the electrical properties of PEDOT/PSS due to excess EG in PEDOT/PSS.[44] The evolution of the volume resistivity of the MWCNT/(EG-PEDOT/PSS) conductive blend with EG loading was similar to that of EG-PEDOT/PSS. Figure 5 clearly demonstrates the interest of the EG treatment as the conductive phase is progressively switched from the MWCNTs to the EG-treated conductive polymer. Initially, the volume resistivity of the pristine PEDOT/PSS film is higher than the volume resistivity of the MWCNT/(PEDOT-PSS) film. So,

dx.doi.org/10.1021/am4011622 | ACS Appl. Mater. Interfaces 2013, 5, 6189–6200

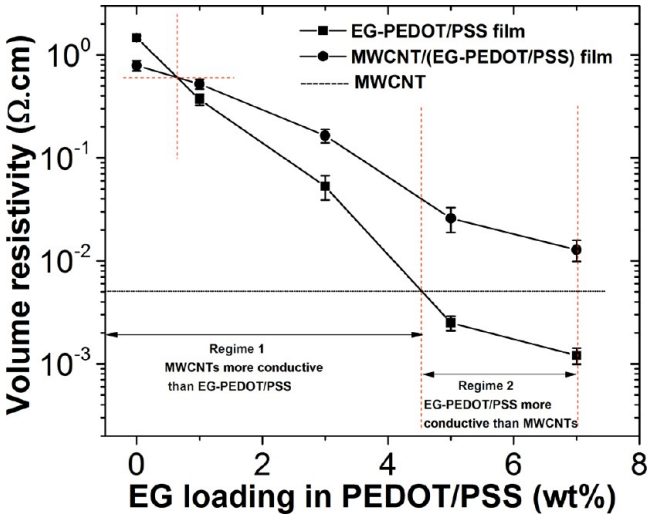

Figure 5. Effect of EG loading on the volume resistivities of the PEDOT/PSS film and the MWCNT/(PEDOT/PSS) film.

MWCNTs act as a classical doping phase that actually enhances the conductivity of the initial bulk PEDOT/PSS. Yet, even for low EG treatment (EG loading in PEDOT/PSS around 0.8%, the crossing point between the two curves in Figure 5), MWCNTs start to have a negative effect and the resistivity of the MWCNT/(EG-PEDOT/PSS) film is increased compared to the resistivity of EG-PEDOT/PSS. The resistivity at the crossing point can be used as a measure of the apparent resistivity of the MWCNT reinforcing phase, which is about 0.6 Ω·cm. This value is much higher than the expected volume resistivity of MWCNTs that, which is expected to be around 5×10^{-3} Ω·cm.[45] The most plausible explanation is that the introduction of MWCNTs in the EG-PEDOT/PSS compound comes with porosity (Figure 4b–e), increasing the apparent resistivity of the MWCNTs. A second explanation, still under investigation, would be the existence of an ohmic interface with relatively high resistance between the MWCNTs and the EG-PEDOT/PSS that would also increase the apparent resistivity of the MWCNTs. The first explanation justifies the use of compression molding in all subsequent nano composite samples to avoid the excessive development of small scale porosity. Second, it is remarkable that the EG-PEDOT/PSS becomes in any case more conductive than MWCNTs (if we assume a reference value of 5×10^{-3} Ω·cm for their volume resistivity) above 4% EG loading. Then, even in a nonporous film, EG-PEDOT/PSS will be the main conducting phase. This kind of material largely differs from classical MWCNT

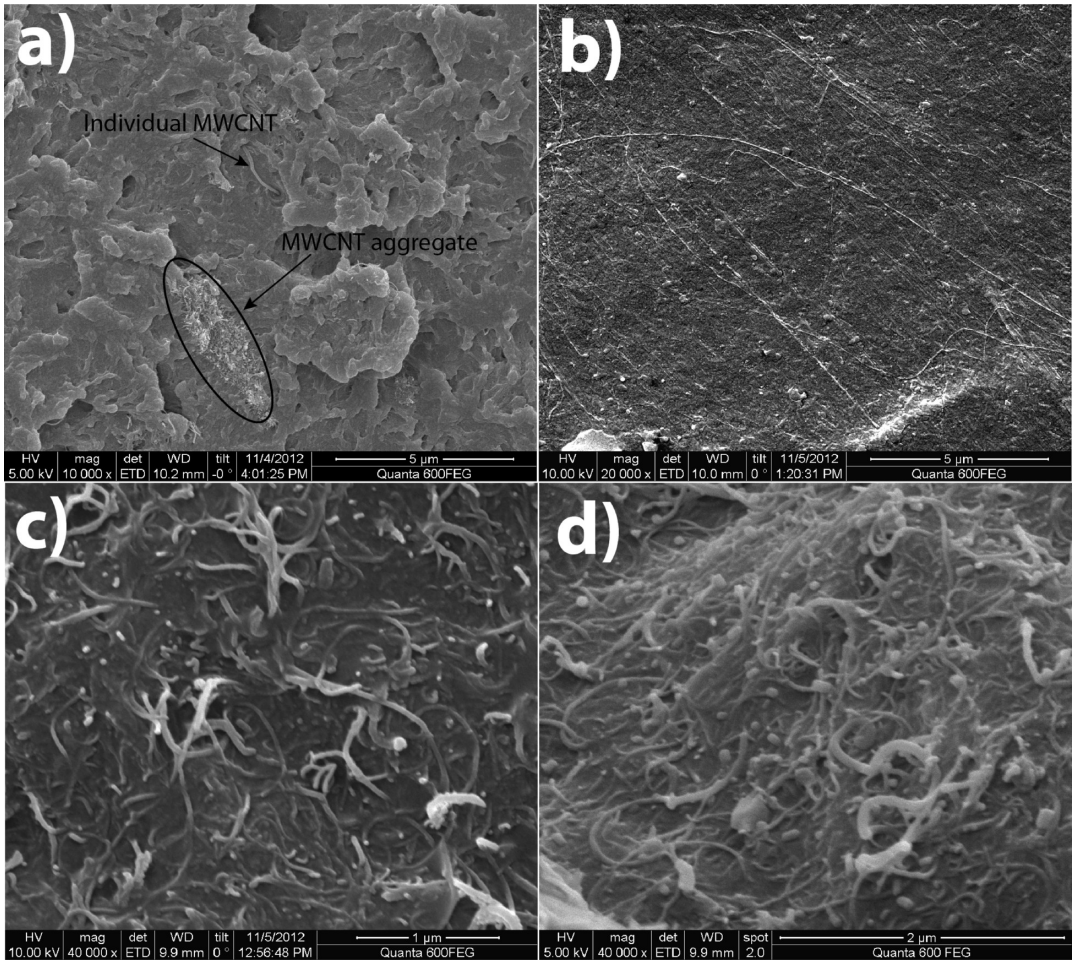

Figure 6. (a) Cryo-fractured surface of the MWCNT/PC nanocomposite (the arrows have been added to indicate individual MWCNT and MWCNT aggregate). (b) Surface mophology of the MWCNT/(EG-PEDOT/PSS)/PC nanocomposite obtained by compression molding (MWCNT loading: 1 wt %). (c, d) Cryo-fractured surface of MWCNT/(EG-PEDOT/PSS)/PC nanocomposites with a MWCNT loading of 1 wt % and 2 wt %, respectively. EG-PEDOT/PSS and MWCNT weight ratio: 1.3:1.

reinforced polymers: MWCNTs are expected here to mainly act as a backbone to ensure the creation of the EG-PEDOT network but will not be the main contributors to the enhancement in conductivity. These results implied that EG plays a major role in enhancing the final electrical properties. To confirm that this conductivity enhancement provided by EG was not endangered by other solvents used in the process, and especially DCM, which is used for dissolving PC, the spin-coated film was immersed in DCM for 2 h. The volume resistivity of this DCM-washed EG-PEDOT/PSS film remained at $(1.04 \pm 0.2) \times 10^{-2}$ Ω·cm, indicating no effect.

Morphology of the Nanocomposites. Figure 6a shows that some aggregates still existed in the MWCNT/PC nanocomposites. The poor dispersion of MWCNTs in DCM results in clustering of MWCNTs. However, on the surface of the MWCNT/(EG-PEDOT/PSS)/PC samples, SEM imaging showed long, curved, and separated MWCNTs embedded in the PC matrix, indicating a good dispersion of EG-PEDOT/PSS coated MWCNTs in the PC matrix (Figure 6b). Figure 6c and d shows SEM images of cryo-fractured surfaces of MWCNT/(EG-PEDOT/PSS)/PC nanocomposites at different MWCNT loadings (1 and 2 wt %). The MWCNTs were apparently well dispersed at the individual level in the PC matrix without obvious MWCNT aggregates.

By comparing Figure 6c and d, we also observe EG-PEDOT/PSS spheres with average diameters of 67 ± 12 nm randomly distributed between the MWCNTs. These EG-PEDOT/PSS spheres were caused by extra hydrophilic EG-PEDOT/PSS liquid in the hydrophobic PC solution. The role of excess EG-PEDOT/PSS leading to highly conductive sphere inclusions in the PC is still not clear, but it probably participates in the creation of the percolated network.

MWCNTs coated with EG-PEDOT/PSS layers in MWCNT/(EG-PEDOT/PSS)/PC (1 and 2 wt %) had average diameters of 41 ± 5 and 43 ± 9 nm, respectively. Due to MWCNT embedment inside the PC matrix, these average values were only obtained by measuring apparent diameters of MWCNTs on the fractured surface. These values are comparable to the observed values in spin-coated MWCNT/(EG-PEDOT/PSS) films if we assume that the gold layer on the PC nanocomposites has a thickness of 3−5 nm.

Figure 7a and b show TEM images of MWCNT/(EG-PEDOT/PSS)/PC (MWCNT: 1 wt %) nanocomposites. It can be seen that the MWCNTs were well dispersed in the PC matrix and exhibited coated EG-PEDOT/PSS layers on their surfaces. The diameter of the coated EG-PEDOT/PSS layers increased with the EG-PEDOT/PSS to MWCNT weight ratio and reached 23.6 ± 3 nm at a weight ratio of 1.3:1 (Figure 7b). This value shows that the presence of coated EG-PEDOT/PSS layers is in good agreement with the results from the above-mentioned TEM characterization of the MWCNT/(EG-PEDOT/PSS) conductive blend (Figure 3b). These layers strongly adhered to the MWCNT surfaces during the solvent mixing process with the PC matrix and also during the compression molding of the nanocomposites. The mass density is equal to 1.2 g/cm^3 for all nanocomposite disks; the unchanged density corresponds to low loading of nanofillers and very low porosity of our nanocomposites disks by compression molding process.

Based on these observations, a possible morphology of the nanocomposites is proposed in Figure 8. In the nanocomposites containing MWCNTs alone (Figure 8a), the MWCNTs are (at best) dispersed randomly, but the conducting pathways are not formed due to insufficient filler content and poor conductivity of the matrix between the fillers. In contrast, Figure 8b illustrates the resulting morphologies of the MWCNT/(PEDOT/PSS)/PC and MWCNT/(EG-PEDOT/PSS)/PC nanocomposites at low PEDOT/PSS loading. The conducting pathways formed after the MWCNTs were coated with the conductive polymer layer. These connected conductive networks strongly affect the electrical properties of the resulting nanocomposites. At higher conductive polymer loading, the excess conductive polymer spheres help to separate the MWCNTs from aggregates and contribute to the overall electrical properties of the nanocomposites (Figure 8c).

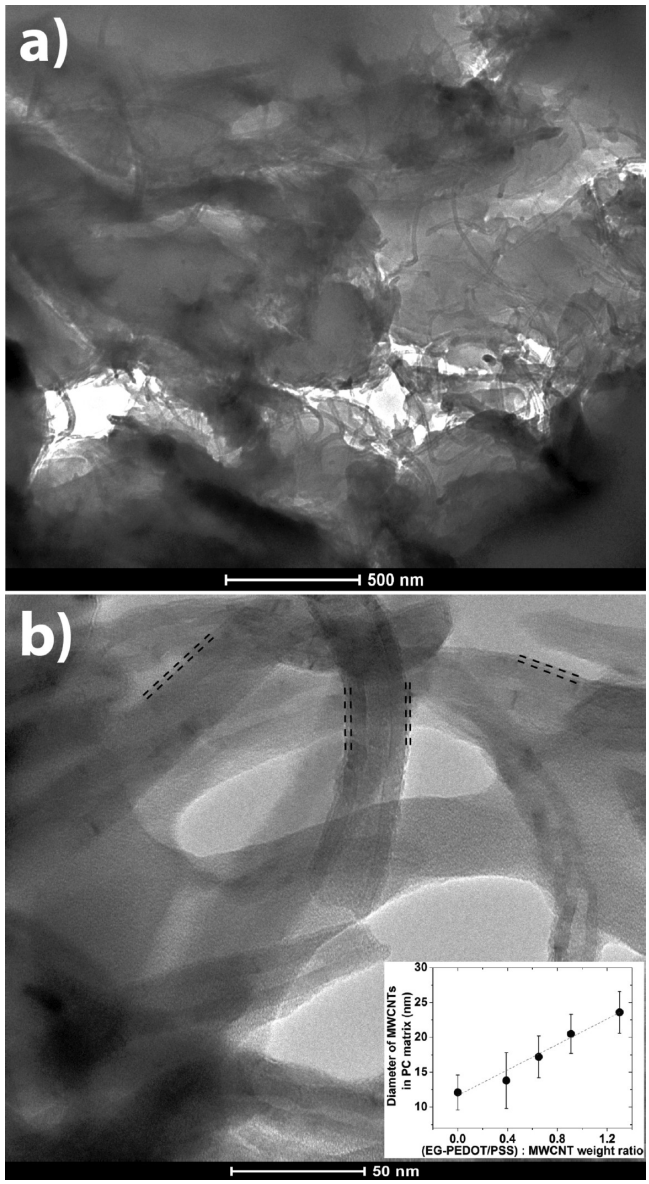

Figure 7. (a) Low magnification TEM images of MWCNT/(EG-PEDOT/PSS)/PC nanocomposites (EG-PEDOT/PSS to MWCNT weight ratio:1.3:1). (b) High magnification TEM images of EG-PEDOT/PSS coated MWCNTs in a PC matrix (the dotted lines have been added as a visual guide to locate the EG-PEDOT/PSS coating; EG-PEDOT/PSS to MWCNT weight ratio:1.3:1). Inset image: the diameter of MWCNTs in PC matrix at different (EG-PEDOT/PSS) to MWCNT weight ratios, MWCNT loading is fixed at 1 wt %.

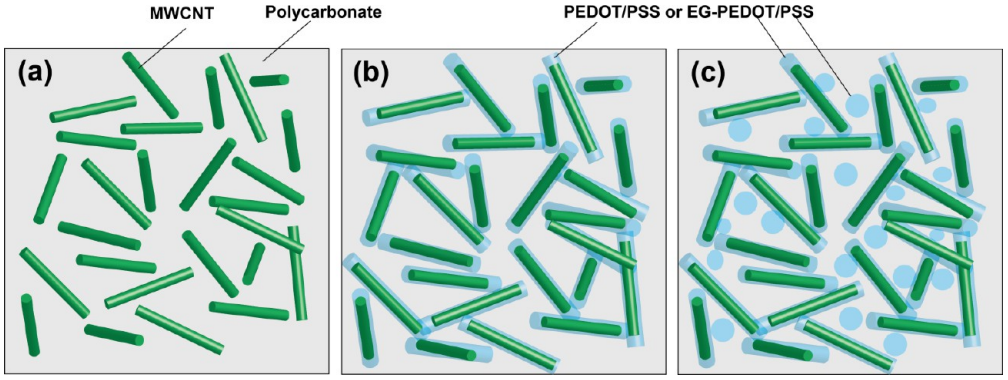

Figure 8. Illustration of (a) MWCNTs in a polycarbonate matrix without connections. (b) MWCNTs in the polycarbonate matrix with connections after functionalization with conductive layer. (c) Excess conductive polymer spheres in a polycarbonate matrix.

Tailoring the Electrical Properties of PC Nanocomposites. Our objective is to obtain a highly tailorable nanocomposite with the desired apparent resistivity. As illustrated in Figure 8, the electrical properties of the nanocomposites studied here can be tailored in three ways: (1) by modifying the MWCNT loading, (2) by adjusting the intrinsic resistivity of the coating layer, and (3) by modifying the thickness of the conductive coating layer. We therefore investigated the effect of each design parameter on the electrical properties.

Effect of MWCNT Loading on Electrical Properties. We first started by tailoring the electrical properties of the nanocomposites by adjusting the MWCNT loading in the matrix. Both the volume and surface resistivity measurements were performed for all nanocomposites. Results are reported in Figure 9 for the different formulations (MWCNT/PC, MWCNT/(PEDOT/PSS)/PC, and MWCNT/(EG-PEDOT/PSS)/PC) as a function of MWCNT loading. As classically observed, the introduction of 1 wt % MWCNTs dramatically decreased both the volume and surface resistivities of the pure PC by up to 8 orders of magnitude to $(1.03 \pm 0.5) \times 10^8$ Ω·cm and $(7.5 \pm 1.3) \times 10^8$ Ω/□, respectively. The percolation threshold of the MWCNT/PC nanocomposites was found to be close to 1 wt % (0.48 vol%). MWCNT/(PEDOT/PSS)/PC and MWCNT/(EG-PEDOT/PSS)/PC exhibited an identical percolation threshold estimated at 0.3 wt % (0.14 vol %). This lower percolation threshold, by comparison to the MWCNT/PC configuration, can be explained by (1) the excellent dispersal of PEDOT/PSS over DCM on MWCNTs and (2) the PEDOT/PSS layer on the MWCNT surface, which modifies the diameter of the nanoparticles (the outer diameter of coated MWCNTs are similar in MWCNT/(PEDOT/PSS)/PC and MWCNT/(EG-PEDOT/PSS)/PC resulting in similar modifications of the percolation behavior for both materials) (Figure 7b).

By modifying the conductivity of PEDOT/PSS with 5 wt % EG, we were able to largely increase the electrical properties of the nanocomposites (Figure 9). A comparison of the electrical properties of the nanocomposites at the percolation loading is shown in Table 2. The volume and surface resisitivity of MWCNT/(EG-PEDOT/PSS)/PC nanocomposites continuously decreased with increasing MWCNT loading until 2 wt %, and reached $(1.3 \pm 0.5) \times 10^5$ Ω·cm and $(1.25 \pm 0.09) \times 10^5$ Ω/□, respectively. Both the volume and surface resistivity were two orders magnitude lower than that of the MWCNT/(PEDOT/PSS)/PC nanocomposite.

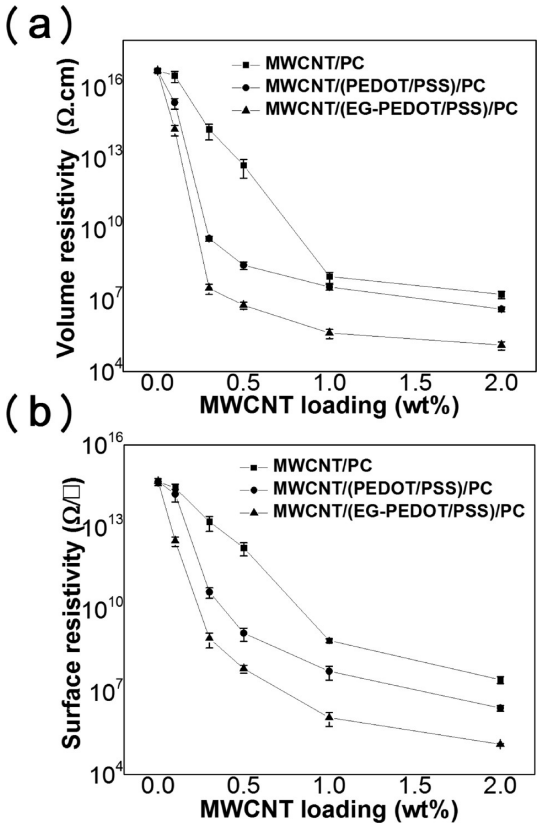

Figure 9. (a) Volume resistivity of MWCNT/PC, MWCNT/(PEDOT/PSS)/PC, and MWCNT/(EG-PEDOT/PSS)/PC nanocomposites as a function of MWCNT loading. (b) Surface resistivity of MWCNT/PC, MWCNT/(PEDOT/PSS)/PC, and MWCNT/(EG-PEDOT/PSS)/PC nanocomposites as a function of MWCNT loading. PEDOT/PSS to MWCNT weight ratio: 1.3:1.

Special care must be given to the values of resistivities when the percolation is well established (MWCNT loading above 1 wt %). The converged volume resistivities for (MWCNT/PC) and (MWCNT/(PEDOT/PSS)/PC) are quite comparable (respective values at 1 wt % MWCNT, $(1.03 \pm 0.5) \times 10^8$ Ω·cm and $(3.7 \pm 1.0) \times 10^7$ Ω·cm; respective values at 2 wt % MWCNT, $(1.8 \pm 0.6) \times 10^7$ Ω·cm and $(4.3 \pm 1.0) \times 10^6$ Ω·cm). Indeed, for pristine PEDOT/PSS, the conductive pattern is still ensured by the MWCNTs (Figure 5), and we cannot expect a remarkable final improvement in conductivity. We only lower the percolation threshold as the PEDOT/PSS

dx.doi.org/10.1021/am4011622 | ACS Appl. Mater. Interfaces 2013, 5, 6189−6200

Table 2. Electrical Properties of PC Nanocomposites at Percolation

samples	surfactant	percolation threshold (wt %)	volume resistivity (Ω·cm)	surface resistivity (Ω/□)
MWCNT/PC	DCM	1	$(1.03 \pm 0.5) \times 10^8$	$(7.5 \pm 1.3) \times 10^8$
MWCNT/(PEDOT/PSS)/PC	PEDOT/PSS	0.3	$(4.2 \pm 1) \times 10^9$	$(4.4 \pm 1.8) \times 10^{10}$
MWCNT/(EG-PEDOT/PSS)/PC	EG-PEDOT/PSS	0.3	$(3.3 \pm 1.5) \times 10^7$	$(9.0 \pm 5.0) \times 10^8$

helps in bridging the MWCNTs together. On the contrary, a very large improvement is observed between (MWCNT/(PEDOT/PSS)/PC) and (MWCNT/(EG-PEDOT/PSS)/PC) that can be associated with the change in mechanisms proposed before: the improvement now comes from the EG-PEDOT/PSS network and confirms the observations of Figure 5.

Effect of EG Loading on the Electrical Properties. We introduced a MWCNT/(EG-PEDOT/PSS) blend into PC by varying the EG loading in PEDOT/PSS (Figure 10). At two

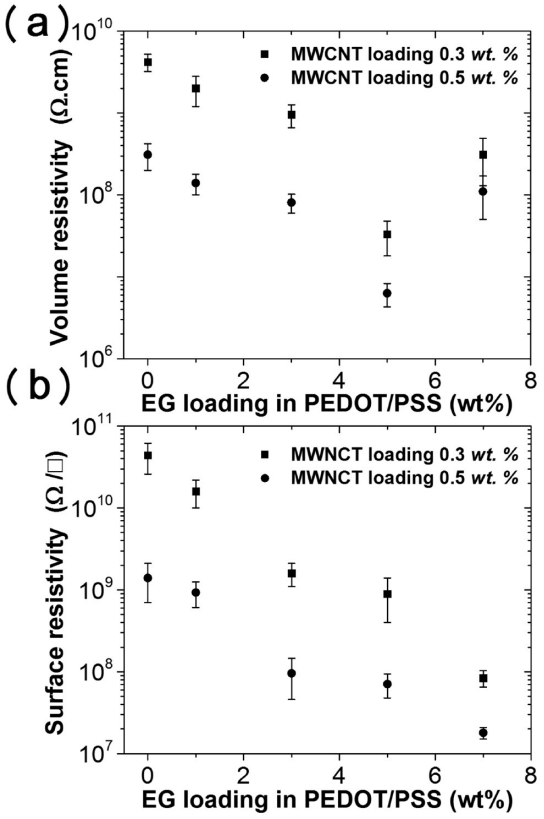

Figure 10. (a) Variation in the volume resistivity with respect to EG loading with fixed MWCNT loadings. (b) Variation of surface resistivity with respect to EG loading at fixed MWCNT loadings. Weight ratio of EG-PEDOT/PSS to MWCNT: 1.3:1.

fixed loadings of MWCNT at 0.3 and 0.5 wt %, we found that the volume resistivity consistently decreased as the loading of EG increase to 5 wt %. At a higher EG loading in PEDOT/PSS (7 wt %), this trend was inverted and the resistivity started to increase again (Figure 10a).

As EG is a nonconductive solvent, this reverse increase in volume resistivity might come from the excessive amount of EG in the PC matrix. To confirm this information, the surfaces of the nanocomposite samples were polished and FTIR was used to characterize the unpolished and polished surface of the MWCNT/(EG-PEDOT/PSS)/PC nanocomposites (Figure 11). For the sample with higher EG loading in PEDOT/PSS (7 wt %), an obvious peak at 1033 cm^{-1} was observed, which is

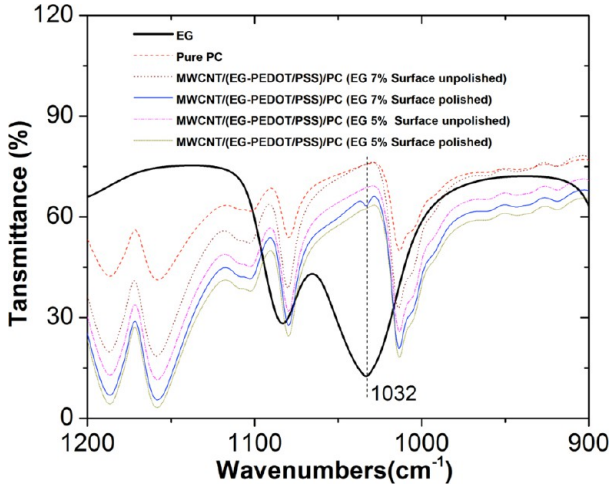

Figure 11. FTIR spectra of EG, pure PC, and MWCNT/(EG-PEDOT/PSS)/PC nanocomposites.

attributed to C−O stretching of EG on the polished surface.[46] However, this peak mostly disappeared on the polished surface with a lower EG loading (5 wt %). On an unpolished surface of both samples, this peak was completely disappeared. This is a strong indication that EG on the surface of the PC matrix can be removed by heating at 240 °C during compression molding. As a result, the surface resistivity of MWCNT/(EG-PEDOT/PSS)/PC nanocomposites consistently decreased as the loading of EG increased to 7 wt %, and the surface resistivity decreased by nearly 1 order of magnitude compared to the case of 5 wt % EG loading (Figure 10b). Due to the different effects of higher loading of EG on the volume and surface resistivity, we could choose different loadings to tailor the volume and surface resistivity.

Effect of EG-PEDOT/PSS Loading on Electrical Properties. As we showed in Figure 4 and the image in the inset of Figure 7b, the thickness of the EG-PEDOT/PSS layers coated on MWCNTs in the MWCNT/(EG-PEDOT/PSS) blend can be modified with different EG-PEDOT/PSS loading. To study this effect, the concentration of EG-PEDOT/PSS was varied while maintaining fixed MWCNT loadings (0.5 and 1 wt %) and a fixed EG loading in PEDOT/PSS (5 wt %). The volume and surface resistivities of MWCNT/(EG-PEDOT/PSS)/PC nanocomposites are shown in Figure 12.

Figure 12 clearly illustrates the role of the thickness of the PEDOT/PSS interface in reducing the percolation threshold. For the MWCNT loading of 0.5 wt % (Figure 8a), the percolation threshold is not established when using the pristine MWCNTs. Adding a small interface (relative weight ratio (EG-PEDOT/PSS):MWCNTs equal to 0.39:1) is enough to create the percolation network and reduces the volume resistivity by 2 orders of magnitude from $(5.2 \pm 3.75) \times 10^{12}$ to $(1.2 \pm 0.75) \times 10^{10}$ Ω·cm and the surface resistivity from $(1.8 \pm 0.9) \times 10^{12}$ to $(1.1 \pm 0.5) \times 10^{10}$ Ω/□. For higher (EG-PEDOT/PSS) loading, conductivity improves as the thickness of the conductive layer increases but in a different regime as the

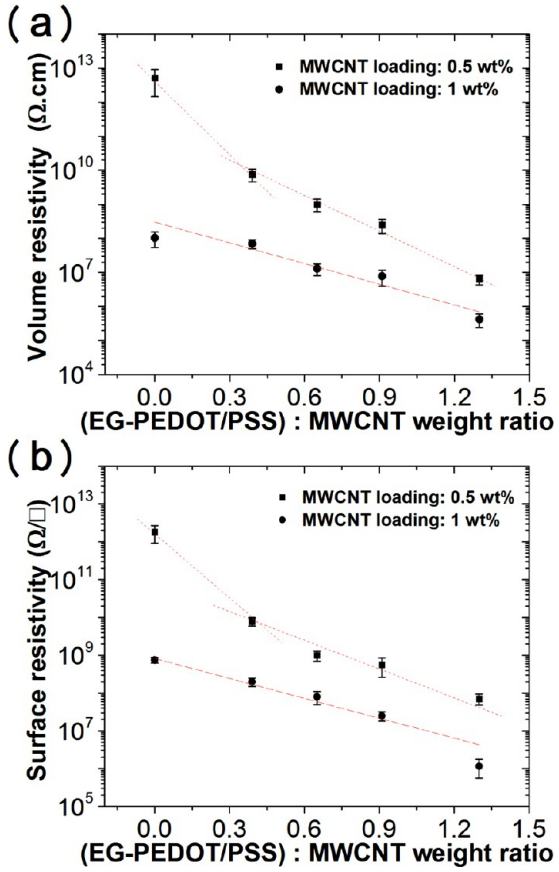

Figure 12. (a) Evolution of the volume resistivity of the nanocomposites when the EG-PEDOT/PSS to MWCNT ratio is increased. (b) Evolution of the surface resistivity of the nanocomposites when the EG-PEDOT/PSS to MWCNTs weight ratio is increased.

percolation network is already formed. On the other hand, at the percolation loading of MWCNT/PC nanocomposites (1 wt %), a conductive network of MWCNTs has already formed even when using pristine MWCNTs. Increasing the loading of EG-PEDOT/PSS into the nanocomposites reduced the resistivity of the nanocomposites, but not as much as in the case of low MWCNTs loading (0.5 wt %).

CONCLUSION

In conclusion, introduction of EG-PEDOT/PSS into MWCNT/PC nanocomposites is an effective way to lower both the percolation threshold and the electrical resistivity. By using EG-PEDOT/PSS to disperse MWCNTs and mixing the resulting conductive blend with PC (MWCNT/(EG-PEDOT/PSS)/PC nanocomposites), we could reduce the volume resistivity and surface resistivity of the nanocomposite by two oders of magnitude compared to that of MWCNT/(PEDOT/PSS) /PC nanocomposites. We confirmed that EG-PEDOT/PSS is strongly adsorbed on the MWCNT sidewalls, and the thickness of EG-PEDOT/PSS can be easily controlled by tuning the EG-PEDOT/PSS and MWCNT weight ratio. These results demonstrate that solvent-treated PEDOT/PSS plays a dominant role in the conducting mechanisms. The conductive polymer becomes the most conductive, with the MWCNTs being in fact only a backbone helping in the dispersion. We hope that our study provides a general reference for tailoring the electrical properties of nanocomposites. Based on these study, more effective electrostatic dissipation and electromagnetic interference materials will be optimized for aerospace structures.

AUTHOR INFORMATION

Corresponding Author

*E-mail: gilles.lubineau@kaust.edu.sa. Tel:+966(2)8082983.

Notes

The authors declare no competing financial interest.

ACKNOWLEDGMENTS

The authors gratefully acknowledge financial support received from KAUST, the BOEING company, and SABIC.

REFERENCES

(1) Hudgin, D.; Bendler, T. *Handbook of Polycarbonate Science and Technology*, 1st ed.; Marcel Dekker Inc: New York, 2000; pp 1−376.
(2) Ezquerra, T.; Martinezsalazar, J.; Calleja, F. *J. Mater. Sci. Lett.* **1986**, *5*, 1065−1066.
(3) Han, M.; Lee, Y.; Kim, W.; Lee, H.; Joo, J.; Park, M.; Lee, H.; Park, C. *Macromol. Res.* **2009**, *17*, 863−869.
(4) Jung, R.; Park, W.-I.; Kwon, S.-M.; Kim, H.-S.; Jin, H.-J. *Polymer* **2008**, *49*, 2071−2076.
(5) Amarasekera, J. *Reinf. Plast.* **2005**, *49*, 38−41.
(6) Baur, S.; E, S. *MRS Bull.* **2007**, *32*, 328−334.
(7) Bandaru, P. *J. Nanosci. Nanotechnol.* **2007**, *7*, 1239−1267.
(8) Baughman, R.; Zakhidov, A.; de Heer, W. *Science* **2002**, *297*, 787−792.
(9) Hussain, F. *J. Compos. Mater.* **2006**, *40*, 1511−1575.
(10) Kumar, S.; Lively, B.; Sun, L.; Li, B.; Zhong, W. *Carbon* **2010**, *48*, 3846−3857.
(11) Sanjinés, R.; Abad, M.; Vâju, C.; Smajda, R.; Mionić, M.; Magrez, A. *Surf. Coat. Technol.* **2011**, *206*, 727−733.
(12) Dror, Y.; Pyckhout-Hintzen, W.; Cohen, Y. *Macromolecules* **2005**, *38*, 7828−7836.
(13) Wang, H.; Zhou, W.; Ho, D.; Winey, K.; Fischer, J.; Glinka, C.; Hobbie, E. *Nano Lett.* **2004**, *4*, 1789−1793.
(14) Tummala, N.; Striolo, A. *ACS Nano* **2009**, *3*, 595−602.
(15) Haggenmueller, R.; Rahatekar, S.; Fagan, J.; Chun, J.; Becker, M.; Naik, R.; Krauss, T.; Carlson, L.; Kadla, J.; Trulove, P.; Fox, D.; DeLong, H.; Fang, Z.; Kelley, S.; Gilman, J. *Langmuir* **2008**, *24*, 5070−5078.
(16) Tsai, Y.; Chiu, C.; Tsai, M.; Wu, J.; Tseng, T.; Wu, T.; Hsu, S. *Carbon* **2007**, *45*, 2823−2827.
(17) Hermant, M.; Klumperman, B.; Kyrylyuk, A.; van der Schoot, P.; Koning, C. *Soft Matter* **2009**, *5*, 878−885.
(18) Hermant, M.; van der Schoot, P.; Klumperman, B.; Koning, C. *ACS Nano* **2010**, *4*, 2242−2248.
(19) Kim, D.; Kim, Y.; Choi, K.; Grunlan, J.; Yu, C. *ACS Nano* **2010**, *4*, 513−523.
(20) Hong, K.; Kim, S.; Yang, C.; Yun, W.; Nam, S.; Jang, J.; Park, C.; Park, C. *ACS Appl. Mater. Interfaces* **2011**, *3*, 74−79.
(21) Yun, D.; Hong, K.; Kim, S.; Yun, W.; Jang, J.; Kwon, W.; Park, C.; Rhee, S. *ACS Appl. Mater. Interfaces* **2011**, *3*, 43−49.
(22) Yun, D.; Rhee, S. *ACS Appl. Mater. Interfaces* **2012**, *4*, 982−989.
(23) Nigro, B.; Grimaldi, C.; Ryser, P. *Phys. Rev. E* **2012**, *85*, 1−8.
(24) Ambrosetti, G.; Grimaldi, C.; Balberg, I.; Maeder, T.; Danani, A.; Ryser, P. *Phys. Rev. B* **2010**, *81*, 1−12.
(25) Ma, Y.; Cheung, W.; Wei, D.; Bogozi, A.; Chiu, P.; Wang, L.; Pontoriero, F.; Mendelsohn, R.; He, H. *ACS Nano* **2008**, *2*, 1197−1204.
(26) Kyrylyuk, A.; Hermant, M.; Schilling, T.; Klumperman, B.; Koning, C.; van der Schoot, P. *Nat. Nanotechnol.* **2011**, *6*, 364−369.
(27) Xia, Y.; Ouyang, J. *ACS Appl. Mater. Interfaces* **2012**, *4*, 4131−4140.
(28) Sun, K.; Xia, Y.; Ouyang, J. *Sol. Energy Mater. Sol. Cells* **2012**, *97*, 89−96.

(29) Zhou, J.; Fukawa, T.; Shirai, H.; Kimura, M. *Macromol. Mater. Eng.* **2010**, *295*, 671−675.
(30) Zhou, J.; Fukawa, T.; Kimura, M. *Polym. J.* **2011**, *43*, 849−854.
(31) Zhou, J.; Gao, Q.; Fukawa, T.; Shirai, H.; Kimura, M. *Nanotechnology* **2011**, *22*, 275501.
(32) Zhou, J.; Kimura, M. *Sen-i Gakkaishi* **2011**, *67*, 125−131.
(33) Ouyang, J.; Xu, Q.; Chu, C.; Yang, Y.; Li, G.; Shinar, J. *Polymer* **2004**, *45*, 8443−8450.
(34) Schroder, D., Ed. *Semiconductor material and device characterization*, 3rd ed.; IEEE Press: Hoboken, NJ, 2006; pp 3−9.
(35) Alemu, D.; Wei, H.; Ho, K.; Chu, C. *Energy Environ. Sci.* **2012**, *5*, 9662−9671.
(36) Lipomi, D.; Lee, J.; Vosgueritchian, M.; Tee, B.; Bolander, J.; Bao, Z. *Chem. Mater.* **2012**, *24*, 373−382.
(37) Ouyang, B.; Chi, C.; Chen, F.; Xi, Q.; Yang, Y. *Adv. Funct. Mater.* **2005**, *15*, 203−208.
(38) Okuzaki, H.; Suzuki, H.; Ito, T. *J. Phys. Chem. B* **2009**, *113*, 11378−11383.
(39) Takano, T.; Masunaga, H.; Fujiwara, A.; Okuzaki, H.; Sasaki, T. *Macromolecules* **2012**, *45*, 3859−3865.
(40) Ouyang, J.; Chu, C.; Chen, F.; Xu, Q.; Yang, Y. *J. Macromol. Sci., Part A: Pure Appl. Chem.* **2004**, *A41*, 1497−1511.
(41) Zhao, L. P.; Li, Y. J.; Liu, Z. F.; Shimizu, H. *Chem. Mater.* **2010**, *22*, 5949−5956.
(42) Han, Y. K.; Chang, M. Y.; Huang, W. Y.; Pan, H. Y.; Ho, K. S.; Hsieh, T. H.; Pan, S. Y. *J. Electrochem. Soc.* **2011**, *158*, 88−93.
(43) Kim, Y.; Sachse, C.; Machala, M.; May, C.; Muller-Meskamp, L.; Leo, K. *Adv. Funct. Mater.* **2011**, *21*, 1076−1081.
(44) Denneulin, A.; Blayo, A.; Bras, J.; Neuman, C. *Prog. Org. Coat.* **2008**, *63*, 87−91.
(45) Ebbesen, T.; Lezec, H.; Hiura, H.; Bennett, J.; Ghaemi, H.; Thio, T. *Nature* **1996**, *382*, 54−56.
(46) Chen, L.; Wan, C.; Wang, Y. *J. Colloid Interface Sci.* **2006**, *297*, 143−150.